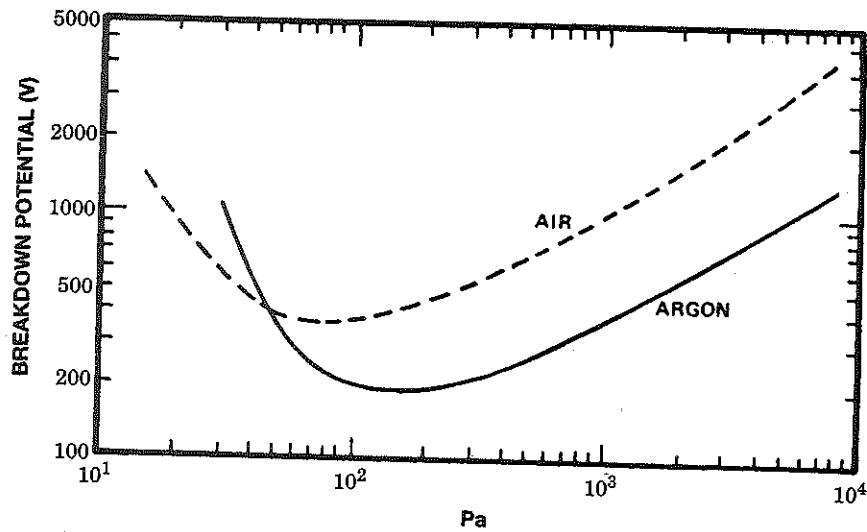

Figure 8.4 Paschen curves for gas breakdown voltage between planar electrodes at spacing d, 293 K. (Source: Reprinted from Ref. 6 by permission. Pressure units changed to Pa.)

netic fields and special techniques of rf electrical power coupling as will be discussed in Chap. 9. For now, the above concepts of electron generation are sufficient to allow us to discuss the narrow-beam vaporization methods of Table 8.1.

8.2 Electron Beams

Here, we describe the use of intense beams of high-energy electrons to evaporate source materials. Electrons thermionically emitted from a hot filament and accelerated into the source material can generate enough energy density to evaporate any material. In a typical case involving 1 A of emission accelerated through a 10-kV voltage drop, 10 kW is delivered upon impact. To avoid dissolving the filament in arriving evaporant, the filament is located out of sight of the evaporant as shown in the electron gun of Fig. 8.5, and the electron beam is pulled around to the surface by a magnetic field, **B**, shown pointing into the figure. The combined force, **F**, on an electron in electric (**E**) and magnetic fields is known as the Lorentz force and is given by

$$\mathbf{F} = \mathbf{F}_E + \mathbf{F}_B = q_e\mathbf{E} + q_e\mathbf{v} \times \mathbf{B} \qquad (8.15)$$

Using SI units, F is in newtons/m^2, q_e in coulombs, **E** in V/m, **B** in webers/m^2 = tesla (1 tesla = 10^4 gauss), and the electron velocity **v** is

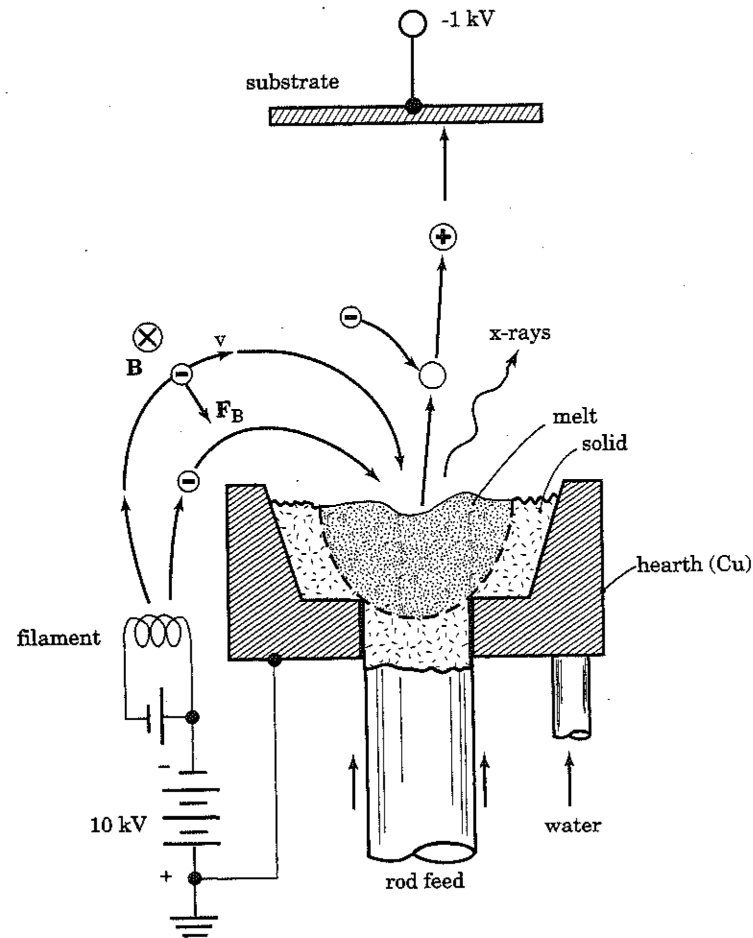

Figure 8.5 Geometry and processes of electron-beam evaporation. Circle with "x" denotes **B** field pointing *into* the paper.

in m/s. The cross-product vector, $\mathbf{F}_B$, is oriented perpendicular to both **v** and **B** as shown in Fig. 8.5, and its sign follows the right-hand-screw rule; that is, rotating **v** toward **B** drives a conventional right-hand-threaded screw in the direction of the vector. Since q_e is negative, $\mathbf{F}_B$ is in the direction shown in Fig. 8.5. The first force term in Eq. (8.15) was encountered in Eq. (6.6); it accelerates the electrons away from the filament or cathode in Fig. 8.5. The **v** so acquired causes the electrons to be deflected sideways as they cross the magnetic field lines, in accordance with the second force term. This second force is balanced by the centrifugal force of the electrons curving at radius r; that is,

$$|q_e \mathbf{v} \times \mathbf{B}| = m|\mathbf{v}|^2/r \tag{8.16}$$

Thus, the "cyclotron" or "Larmor" radius of an electron orbiting in a magnetic field is

$$r_c = m_e v_\perp / q_e |\mathbf{B}| \tag{8.17}$$

where $v_\perp$ is the component of $\mathbf{v}$ that is perpendicular to $\mathbf{B}$. For example, using SI units and numbers typical of electron-beam evaporation sources, an electron after accelerating through a 10 kV potential drop has $\mathbf{v} = 5.9 \times 10^7$ m/s by Eq. (8.7). In a field of 10^{-2} webers/m^2 (100 gauss), this gives $r_c = 0.034$ m = 3.4 cm. The behavior of electrons in magnetic fields will also be important in understanding magnetically confined plasmas (Chap. 9). In the electron-beam source, $\mathbf{B}$ is generated either by a permanent magnet or a solenoid coil mounted below the source. Modulation of the solenoid field can be used to steer the electron beam.

It is important to aim the beam at the center of the source material and to avoid hitting the material's container (the "hearth"). However, deposition uniformity is improved by scanning the beam around on the surface in a raster pattern using the above solenoid coil along with a second lateral steering coil. Without rastering, the evaporating material tends to be angularly distributed in a lobe-shaped pattern approximated by $\cos^n\theta$ with n = 2 to 4, rather than following a cosine distribution (n = 1; see Fig. 4.12). The lobe is apparently due to collimation arising from the depression created in the surface by rapid evaporation from the point of beam impact. This collimation occurs even with molten metals, whose viscosity is so high that flow of the melt into the depression may not be able to keep up with the evaporation rate. Even with rastering, evaporation rate and flux distribution fluctuate much more than in joule-heated crucibles. Therefore, when rate control is important, vapor flux monitoring with feedback control to the filament power should be used (see Sec. 4.7).

The source material is usually contained by a Cu "hearth" which is water-cooled to prevent its outgassing or melting. Cooling also prevents the hearth from alloying with molten source materials, because the material immediately adjacent to a cooled hearth cannot melt. Then, the source material is essentially being evaporated from a crucible formed by its own solid phase, and this makes electron-beam evaporation particularly useful for materials like Si, which alloys with everything it touches when it is molten. When there does exist a crucible material that will not contaminate the melt, it can be used as a hearth liner to reduce heat-sinking and thereby increase evaporation efficiency. Even electrically insulating source and crucible materials can be used, because usually the secondary-electron yield from beam impact is greater than unity at the high energy used, so that negative charging of the surface is avoided. The localized melting also allows the continuous feeding of a solid bar of source material up through the bottom of the hearth, so that an enormous quantity of material can be evaporated before reloading is needed, such as a 5-cm-diameter by 20-cm-long bar. The bar feed rate can be feedback-controlled based on the monitored evaporation rate, so as to keep the melt surface at a constant height. In the case of alloys, rod-feeding has the further advantage that evaporating composition has to be equal to rod composition in steady state. The transient approach to steady-state melt composition was analyzed in Sec. 4.3. The time to reach steady state can be greatly reduced by starting with a hearth charge which matches the steady-state melt composition rather than one which is the same as the rod composition.

All evaporation done with narrow, intense energy beams is subject to the "macroparticle-spitting" problem. This problem occurs even with joule-heated crucibles, as discussed in Sec. 4.5.1, but it is much more severe with energy beams. One mechanism of macroparticle ejection common to all vaporization methods and dominant for electron beams is the sudden evaporation of a nodule of a particular contaminant whose vapor pressure is much higher than that of the source material. This sudden pressure burst can knock from the surface a macroparticle of solid or liquid material typically 0.1 to 1 μm in diameter. The particle is likely to land on the depositing film, where it is most unwelcome. The velocities of such particles are high enough that they are negligibly affected by gravity over the transport distance. However, many of the particles are charged in the case of Si and probably in general, and these reportedly [7] can be deflected effectively using a transverse $\mathbf{E}$ field applied from an electrode placed off to the side at ±4 to 6 kV.

The volatile contaminant nodule which ejects the macroparticle may be an inclusion in the solid source material, a gas pocket trapped within "sintered" material (that is, hot-pressed powder), or a "slag" accumulating on the surface of molten metal by reaction of background gases with the metal or by precipitation of bulk contaminants upon melting of the metal. The macroparticle problem is minimized by using very pure source material, preferably manufactured by melting rather than by sintering. Vacuum-melted charges shaped to fit most commercial electron-beam hearths are available from materials suppliers. In the cathodic-arc-evaporation and laser-ablation methods to be discussed in the following sections, there arise other macroparticle-ejection mechanisms that are much less easily counteracted. The problem does not occur in sputtering because the energy density at the sur-

face is much lower, although at background pressures above 20 Pa or so, particles can form in the *gas* phase (more on this in Sec. 9.6.2).

Although electron-beam evaporation is a thermal process, so that the vapor atoms leave the surface with only thermal energy of ~0.2 eV, several kinds of nonthermal energy still arrive at the film surface. One is **x-rays** generated by electron-beam impact on the source material, which is, after all, the operating principle of the x-ray tube. The x-rays generated by a 10-keV electron beam are not "hard" enough (energetic enough) to penetrate the vacuum-chamber wall or window to become a hazard to the operator, but they can be a hazard to the product. In particular, dielectric materials for electronic applications can develop undesirable charge-trapping defects or embedded charge from x-ray irradiation, and it is not always possible to anneal out this damage afterwards. A dielectric material underlying the film being deposited can also be damaged.

The second form of nonthermal energy accompanying electron-beam evaporation is a beneficial one. **Positive ions** are generated above the source by impact of the incoming beam upon the outgoing vapor, as shown in Fig. 8.5. The fraction of vapor ionized varies with beam density and vapor composition and is of the order of 0.01 to 0.1. These ions cannot get drawn into the cathode filament despite its negative bias, because the cyclotron radius of a particle increases as $\sqrt{m}$ in accordance with Eqs. (8.7) and (8.17) and is therefore hundreds of times larger for ions than for electrons. On the other hand, by biasing the substrate negatively as shown in Fig. 8.5, the ions *can* be accelerated into the depositing film. Because the resulting energy flux can be very large, it can have a profound effect on film structure even though the fractional ionization of depositing vapor is small—a fact which applies to all of the deposition techniques that involve ions. The effects of ion bombardment on film structure will be discussed in Sec. 8.5. This acceleration technique is known as "ion plating" by analogy to electroplating from liquid solution; but the term is misleading, because the ions are just modifying the deposit rather than constituting the dominant depositing species as they do in electroplating. Among the vapor-phase thin-film processes, ions are the dominant depositing species only with cathodic arcs and sometimes with high-intensity glow discharges.

Sometimes, a gaseous source species is introduced into the evaporation chamber for the purpose of forming a compound film by reaction with the evaporating species. The gaseous species will also become partially dissociated and ionized by collisions both with the electron beam and with the vapor ions if they are being accelerated toward the substrate. The ionized gas forms a plasma between the source and the substrate. This **gas activation** assists the compound-film-formation reaction and is therefore a form of "activated reactive evaporation," which will be discussed further in Sec. 9.3.2. Similar gas activation occurs in any process in which a plasma is present, and techniques other than electron-beam evaporation actually allow much higher reactant-gas pressure, because the problem of electron-beam scattering is not present.

It is important to keep in mind that in *any* of the energy-enhanced processes, the background gases in the vacuum chamber also become activated and thus become incorporated more easily into the film as contaminants. This means that the vacuum-cleanliness practices of Sec. 3.4 are even more important to observe in energy-enhanced processes than in thermal processes whenever incorporation of the background gases would degrade the film.

8.3 Arc Plasmas

The remaining energy-enhanced techniques to be discussed in this book all involve a plasma of some sort. The general concept of a plasma was introduced at the beginning of this chapter. To put the arc type of plasma into perspective, refer to Fig. 8.6, which distinguishes dc (direct-current)-discharge plasmas according to several factors; namely, the voltage drop between anode and cathode, the total current being passed between electrodes, and the current density at the cathode. It is important to know where one is operating on this map in order to control a plasma-deposition process. In dc plasmas, the current is controlled to the desired position on the map by using a current-limited power supply. The values of voltage and current shown are typical only and will vary considerably with gas composition and pressure, electrode material, and geometry. Starting in the shaded region at the left of the figure, very small amounts of current are passed even before a plasma is ignited, due to field emission and to photoemission induced by stray light. If current and voltage are allowed to increase, electron avalanching eventually occurs in the intervening gas and causes breakdown, as was discussed at Fig. 8.2. Breakdown takes the form of a spark at high pressure ($>10^4$ Pa or so) and takes the form of a much more diffuse "glow" at lower pressure. After breakdown, the plasma has been "ignited," and a continuous flow of electrons and ions between electrodes is sustained by electron-impact ionizing collisions in the gas phase, as shown in Fig. 8.2 and Eq. (8.14). In the self-sustained dc glow discharge, the electrons that initiate the avalanching are generated by secondary-electron emission induced by ion bombardment of the cathode. [Plasmas driven by *rf*

there is some loss of vapor flux and deposition rate. Moreover, merely keeping the film out of the line of sight of the cathode is not sufficient, because the macroparticles seem to be able to reflect from duct surfaces and still reach the film unless baffles are also incorporated into the duct walls to scatter the particles [14].

Arc deposition can also be operated in a **gas ambient**. One use of the gas is to scatter vapor ions as they approach the substrate so that they arrive from a wide range of angles and can thus coat complex-shaped substrates such as tool bits more evenly, at least in *cathodic-arc* deposition where ionization fraction is near unity. The ability to coat oblique or hidden surfaces is called "throwing power" in reference to the same feature of some electroplating processes. The same scattering would occur for *thermal* evaporation into a gas ambient, but there the vapor tends to condense into particles in the gas phase due to collisional cooling, whereas ions are prevented from doing so by their mutual repulsion. Gas-phase condensation was discussed in Sec. 4.5.4.

The second use of a gas ambient is for compound-film formation. The stream of electrons and ions emanating from the arc activates reactive gases enough so that full reaction of the metal vapor to stoichiometric compound films can be achieved. Thus, metal carbides, nitrides, and oxides can be formed [15] using CH_4, N_2, and O_2 at pressures of 1 to 100 Pa. TiN is a particularly useful wear-resistant coating because of its hardness, low coefficient of friction, and chemical inertness. Many other plasma processes also may be used to deposit compounds reactively from metal sources. For example, reactive glow-discharge sputtering is widely used because of its combination of high deposition energy, freedom from macroparticles, and ability to uniformly coat large areas. However, special control techniques must often be employed there to obtain stoichiometric films because of an inherent instability in the degree of cathode-surface "poisoning" by the reactive gas (more on this in Sec. 9.3.3). Arc sources do not exhibit the poisoning effect, because the evaporation *flux* (atoms/cm^2·s) is much higher than in sputtering due to the much higher power density, and this flux is much higher than the arrival flux of reactive gas. This behavior and the high ionization fraction are the two principal advantages of arc sources.

8.4 Pulsed Lasers

The use of a pulsed UV laser beam for vaporizing solid source material constitutes the last of the narrow-beam vaporization techniques of Table 8.1 to be discussed. High-power lasers, such as the Nd:YAG at a wavelength of $\lambda = 1.06$ μm and the CO_2 at 10.6 μm, have long been used for cutting and drilling very hard or refractory materials. Because much of the material ablates as macroparticles rather than vaporizing as atoms or molecules, "laser ablation" has received much less attention for thin-film deposition than have other vaporization techniques. However, recent work has demonstrated that very good "high-T_c" superconducting ceramic thin films can be deposited by pulsed UV-laser vaporization in an O_2 ambient (Hubler, 1992), and this has generated considerable interest in developing the technique further for film deposition. A typical high-T_c material is "1,2,3-YBCO," a mixed oxide of the approximate composition $(Y_2O_3)_{0.5}(BaO)_2(CuO)_3$. Obtaining a high superconducting-transition temperature, T_c, requires close composition control, and a key advantage of the pulsed UV beam is that it can achieve congruent evaporation of these complex materials. This advantage is shared by sputtering, and when a glow discharge is used for sputtering rather than an ion beam, one can also operate in the 50 Pa or so of O_2 ambient which is required to prevent substoichiometric O content in the YBCO. However, fast O^- ions ejected from the sputtering cathode damage the film's crystallography, and it is difficult to eliminate these ions (more on this in Sec. 9.3.3). On the other hand, sputtered films are free of macroparticles. With effort, reasonably good superconducting films have been deposited by both techniques. This is a classic example of the trade-offs involved in choosing a deposition technique, and it emphasizes the need to carefully examine all of the advantages and drawbacks of each one.

Congruent evaporation by a pulsed UV laser results from the deposition of an intense energy pulse in a shallow depth of the source material and a consequent explosive evaporation of a thin layer before it has time to disproportionate. The depth involved is either the optical absorption depth, $1/\alpha_r$, or the thermal diffusion length, Λ, whichever is larger. Recall that α_r is the optical absorption coefficient from Eq. (4.49). Taking a typical example, $\alpha_r = 10^5$/cm and $1/\alpha_r = 100$ nm for YBCO at the KrF excimer laser λ of 248 nm. For Λ, we may define a thermal diffusion length by analogy to the mass diffusion length of Eq. (5.25):

$$\Lambda = 2\sqrt{\alpha t} \qquad (8.19)$$

where α is the thermal diffusivity from Eq. (8.18). Λ is a measure of how deep into the material the depositing energy penetrates during the length of the pulse, t. Taking handbook data for BaO at room T, we find $\alpha = (4\ \text{W/cm·K})/(6.5\ \text{g/cm}^3)(0.31\ \text{J/g·K}) = 2.0\ \text{cm}^2/\text{s}$. Then, for a typical pulse length of t = 20 ns, we find $\Lambda = 4000$ nm, which is much larger than $1/\alpha_r$ for YBCO, so that thermal diffusion determines the

energy deposition depth for this case. For poorer thermal conductors or more transparent materials, $1/\alpha_T$ can determine depth. To achieve the goal of shallow energy deposition, one wants both a fast pulse and a high α_T. For nonmetals, high α_T requires λ to be below the fundamental absorption edge of the material, as discussed following Eq. (5.58). Also for nonmetals, α_T increases well above its initial value when successive pulses are delivered to the same area of the surface. This is because the pulse imparts a "thermal shock" to the material, as discussed later in connection with macroparticle ejection. The shock damages the near-surface region crystallographically [16, 17] and thereby increases α_T. This phenomenon causes evaporation rate to increase with time during initial evaporation from a fresh target.

For the deposited energy to result in evaporation, there must be enough of it to first heat the material to a T of high vapor pressure, p_v, and this heat may also involve the heat of fusion ($\Delta_c H$) consumed in melting the material. Then, the heat of evaporation, $\Delta_v H$, must be supplied. Since the pulse repetition rate is very low, say 10 pulses/s, the material may be assumed to have completely cooled between pulses. A typical excimer pulse delivers 0.2 J into a 0.1-cm^2 area, corresponding to a "fluence" of 2 J/cm^2. Note that this represents a time-average power of only 2 W (J/s), 10^3 lower than in evaporation with the other Table 8.1 beams. Evaporation is possible with such low power only because the *instantaneous* power density is very high:

$$(2\ \mathrm{J/cm^2})/(20\ \mathrm{ns}) = 10^8\ \mathrm{W/cm^2}$$

which approaches that of the cathodic arc. Now, heating a BaO volume of 0.1 cm^2 $\times$ Λ to, say, its boiling point (p_v = 1 atm) of 2000 K requires 0.11 J, leaving 0.09 J for supplying $\Delta_c H$ and $\Delta_v H$. That is, 0.11 J is the *threshold* pulse energy for laser vaporization in this example. Since for BaO, $\Delta_c H + \Delta_v H$ = 437 kJ/mol = 1.9×10^4 J/cm^3, a thickness of 480 nm can be evaporated with this remaining 0.09 J. In practice, an evaporated depth of tens of nm is more typical [17], because much of the beam energy is either reflected from the surface or absorbed by the vapor cloud which forms over it.

Figure 8.9 shows the geometry for pulsed laser evaporation. The beam enters the vacuum chamber through a quartz window and is directed at the target of source material at an oblique angle so that the substrate can be placed directly facing the target surface. This is done because most of the evaporant is directed in a narrow lobe oriented closely perpendicular to the target, for reasons to be discussed below. Usually, the beam is scanned in a raster pattern so that the target erodes evenly. The delivery of vaporization energy in fast pulses allows two pulse-synchronized devices to be incorporated. One is a spinning polygon having a different source material on each face so that alternating-layer structures or multi-element composition control can be obtained [18]. Here, the switching time between materials is limited only by the laser pulse rate, so it can be much shorter than switching done with mechanical shutters in MBE or sputtering, or with gas valves in CVD. For applications such as superlattices, however, the close control of deposit thickness which is required can be difficult to achieve because of fluctuation in pulse energy, drifting target-surface condition, and the nonuniform deposit obtained from the narrow lobe of evaporant. The second pulse-synchronized device is a spinning disc containing an aperture synchronized to the pulses, to filter out macroparticles ejected from the target. Since the macroparticles travel much more slowly than do the vapor atoms, they can be selectively blocked by the disc. However, the hardware and geometry are awkward and not completely effective, so it would be better to avoid generating the macroparticles in the first place. Another practical problem in laser vaporization is deposition of evaporant on the beam window. When one is using a gas ambient at a pressure up in the fluid-flow regime [Kn << 1 in Eq. (2.25)], such as 100 Pa, admitting the gas

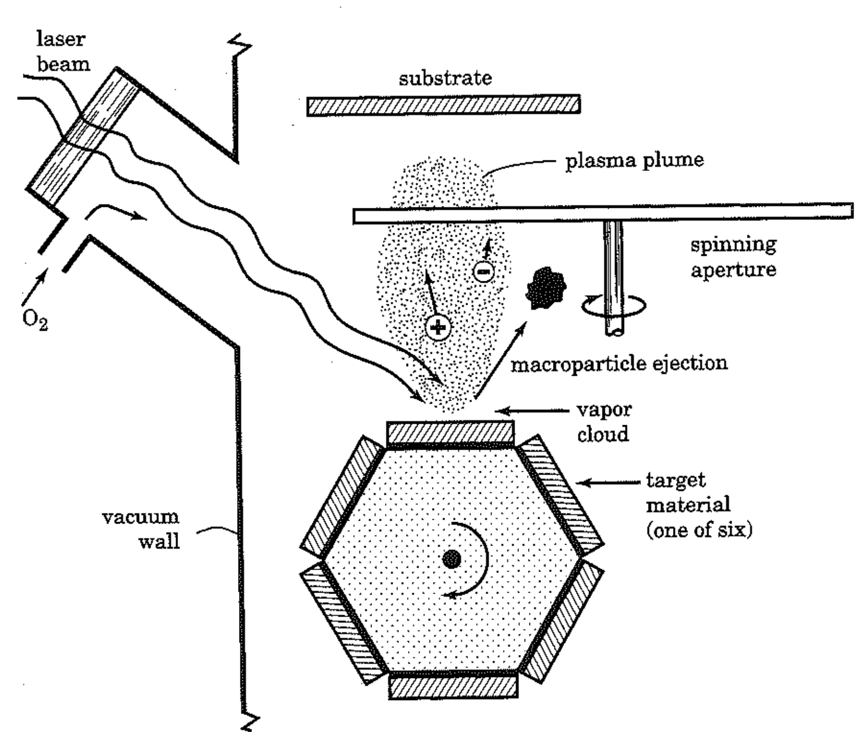

Figure 8.9 Geometry and processes of pulsed-laser vaporization.

at the window as shown in Fig. 8.9 will sweep approaching vapor away from it as described by Eq. (3.13) for the oil backstreaming problem.

Two evaporant components have been observed [19]. One has the $\cos\theta$ distribution of Fig. 4.12, has thermal energy, and tends to be nonstoichiometric, as in conventional thermal evaporation. The other has a sharply lobed $\cos^n\theta$ distribution, with n variously reported in the range of 4 to 14. The lobed component is closely stoichiometric and has a velocity of $\sim 10^4$ m/s [20], which is way above thermal velocity and corresponds to a particle energy of ~40 eV by Eq. (8.6) using typical atomic masses. This kinetic energy is a key feature of pulsed laser evaporation. It can be transported in vacuum to the film to modify its structure, or it can be used to activate reaction with a gaseous ambient such as O_2 by collisional dissociation of the gas molecules. When a gas ambient is used, the thermal vapor component can condense in the gas phase into unwanted particles (see Sec. 4.5.4), whereas the lobed component seems not to do so because of its high energy. The fraction of undesired thermal component becomes small when pulse energy is well above the threshold level discussed earlier, so that there is excess energy available to accelerate the vapor.

The mechanism of vapor acceleration has been likened to supersonic expansion from a high-pressure nozzle [20, 21], which was discussed in Sec. 4.5.4. Explosive evaporation of a layer of material by the fast pulse produces a volume of hot, high-pressure vapor calculated to be about 50 μm thick [21] and covering the much wider irradiated area of ~ 0.1 cm^2. Absorption of incoming light by the vapor raises the T and pressure still further. Most of the expansion of this vapor volume will be in the direction of steepest pressure gradient and largest cross-sectional area—that is, perpendicular to the surface—and this produces the sharp lobe. Vapor collisions during expansion convert thermal energy into directed kinetic energy as in the supersonic nozzle, resulting in the narrowed and upward-shifted velocity distribution characteristic of supersonic beams [20].

A plasma forms in the vapor plume both from thermionic electron emission from the hot surface and from photon absorption by the vapor [21]. The 5-eV energy of a 248-nm photon [from Eq. (6.5)] is not enough to ionize most vapor atoms. However, at high light intensity, additional photons can be absorbed by the same atom before the electronically excited state created by the first one has time to relax, and thus the ionization energy can be acquired by multiphoton absorption [22]. Indeed, one of the most dramatic phenomena exhibited by high-power lasers is electrical breakdown in air observed as a tiny spark suspended in space at the focal point, accompanied by a sharp "crack" noise. In pulsed laser evaporation, the plasma appears instead as the glowing plume shown in the cover photograph of this book. The gradations in color result from the decreasing level of electronic excitation in the vapor and gas atoms at positions further from the source. This plasma has two benefits. Gaseous reactants become dissociated and ionized, and this assists their reaction with the depositing vapor. Also, the ions can be accelerated into the film by application of negative bias to the substrate as in the other energy-beam techniques.

Macroparticle ejection is a serious problem in pulsed laser vaporization. It is reduced by using pure and nonporous materials as discussed in Sec. 8.2; but this does not eliminate the problem, so other ejection mechanisms must be operating. One possibility is excess subsurface heating, which we discussed also for the cathodic arc. Generation of heat throughout the light-absorption depth of $1/\alpha_r$, coupled with surface evaporative cooling, can lead to a ratio of subsurface T to surface T, $\theta = T/T_o$, which is above unity, as shown in Fig. 8.10. There, θ is plotted versus dimensionless depth, $S = \alpha_r z/B$, for various values of the parameter $B = \alpha \cdot \alpha_r \Delta_v H/V_m I$, where z is linear depth, α is the thermal diffusivity from Eq. (8.18), $\Delta_v H/V_m$ is the heat of evaporation per cm^3 (J/mol ÷ cm^3/mol), and I is the instantaneous power density, typically 10^8 W/cm^2. The plot is for $1/(1+\lambda) = 0.7$, where $\lambda = c_p T_o/\Delta_v H$. The quantity $1/(1+\lambda)$ varies little among materials, being 0.67 for Al_2O_3 and 0.82 for Cu and BaO. Now, the Fig. 8.10 solution is a steady-state one involving continuous-wave (CW) laser energy input and continuous evaporation and retreat of the surface, z being measured from the retreating surface. Since a 20-ns pulse cannot be considered steady state, Fig. 8.10 can give only a qualitative indication of T behavior during the pulse. Using the physical properties of BaO at room T and using $\alpha_r = 10^5$/cm for YBCO as before, we find B = 37, which would re-

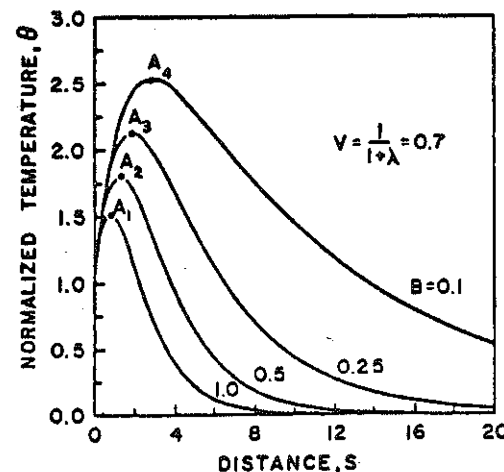

Figure 8.10 Steady-state T vs. depth in a material being laser-vaporized. Parameters are defined in text. (Source: Reprinted from Ref. 23 by permission.)

sult in a maximum T/T_o close to unity. However, several factors could lead to substantially lower B and increased likelihood of macroparticle ejection by subsurface vapor pressure; these include lower thermal conductivity and diffusivity (α), lower optical-absorption coefficient (α_r), and higher pulse energy (I).

Another possible ejection mechanism is "thermal shock." Heating of the near-surface region causes it to want to expand in accordance with its thermal expansion coefficient, α_T (Sec. 5.6.1), and this leads to a compressive-stress transient that propagates as a shock wave through the material. This wave reflects off the surface because of the large acoustic-impedance mismatch to the vapor phase, just as light reflects off a boundary of refractive-index difference. The returning wave causes a *tensile* stress transient in the material, as shown in Fig. 8.11 for stress given in bars (= 10^5 Pa). This particular stress transient was calculated and measured for Corning CS756 glass receiving a 28-ns pulse of 0.08-J/cm^2 fluence from a ruby laser at λ = 694 nm where α_r = 65/cm for this glass. This "thermoelastic" stress is predicted [24] to scale linearly with fluence and α_r, as one would expect, so extrapolating from Fig. 8.11 to the previously discussed case of YBCO receiving 2 J/cm^2 with $\alpha_r = 10^5$/cm, we predict a peak tensile stress of 15 GPa. This is well above typical tensile strengths of 1 GPa (Sec. 5.6.1), so this appears to be a likely mechanism for macroparticle ejection.

8.5 Ion Bombardment

The impingement of energetic ions or atoms upon a solid surface produces a wide variety of effects, and there has been a vast amount of experimental and theoretical work on the subject. Many of these effects are beneficial to thin-film deposition, and those that are not can usually be avoided by controlling ion composition and keeping

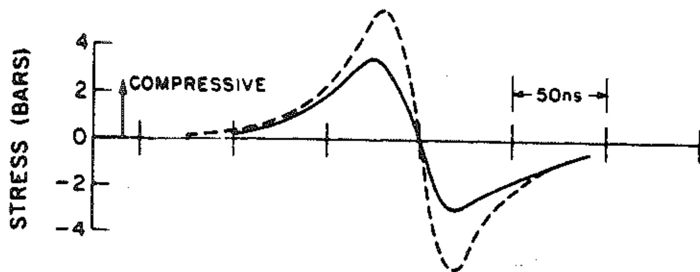

Figure 8.11 Measured (solid line) and calculated (dashed line) stress waveforms in glass resulting from a laser pulse, for conditions described in the text. Sign of stress here is opposite from conventional (see Fig. 5.30). (Source: Reprinted from Ref. 24 by permission.)

energy low. Thus, ion bombardment is one of the most important thin-film process parameters, and we will discuss it here in considerable detail. Energetic ions and atoms have similar effects on the solid, and reference to ion bombardment in this text is meant to include energetic atom or molecule bombardment. By the way, since ions can be focused into submicron-diameter beams, metal-ion beams can be used directly to deposit thin films in fine patterns. However, this is a very specialized technique and will not be discussed further here.

The effects of ion bombardment on a material differ substantially from those of electron and photon bombardment because the ion mass is of the same order as the mass of the atoms in the bombarded solid. Consider a head-on, binary, elastic collision between an impinging particle of mass m_i and energy E_i and a target particle of mass m_t which is initially at rest. The amount of kinetic energy transferred to the target particle is called the "recoil" energy and is traditionally labeled T_m for the head-on case. Conservation of energy and momentum require that

$$\boxed{T_m = \frac{4m_i m_t}{(m_i + m_t)^2} E_i = \gamma_m E_i} \tag{8.20}$$

If the impinging particle is a 10-keV electron ($m_i = 9.1\times10^{-31}$ kg) and the target is a Ni atom [m_t = 59 u (atomic mass units) $\times$ 1.67×10^{-27} kg/u], then T_m = 0.37 eV, which is enough to heat up the Ni atom but much less than enough to dislodge it from its lattice site. T_m is even lower for photons. At the other extreme, if $m_i = m_t$, then *all* of the energy is transferred to the target, as billiards players know. If the masses are within $\times$2 of each other, then $\gamma_m > 0.9$.

This efficient energy transfer to individual atoms is the key feature of ion bombardment. It gives ions the ability to *move atoms around*, and all of the many effects of ion bombardment on film structure and properties arise from this one fact. When $m_i \sim m_t$, an E_i of only a few eV is enough to move a target atom from one surface site to another or to dissociate a molecular impinging ion into reactive fragments. An E_i of only a few tens of eV is enough to displace a surface atom into the bulk of the solid or to dislodge a near-surface atom into the vapor phase. The latter process is known as sputtering, which is widely used for generating source vapor by bombardment of a target at a keV or so using ion beams or glow-discharge plasmas. The sputtered particles themselves have kinetic energies of several eV, and this energy strongly affects film structure. High kinetic energy of the depositing material also occurs in many other deposition processes (Secs. 4.5.4 and 8.2–8.4), and this situation is generally known as "energetic con-